CHEMISTRY
A EUROPEAN JOURNAL

A Density Functional Study on a Biomimetic Non-Heme Iron Catalyst: Insights into Alkane Hydroxylation by a Formally HO−Fe^{V}=O Oxidant

Arianna Bassan,*[a] Margareta R. A. Blomberg,[a] Per E. M. Siegbahn,[a] and Lawrence Que, Jr.[b]

Abstract: The reactivity of [HO−(tpa)Fe^{V}=O] (TPA = tris(2-pyridylmethyl)amine), derived from O−O bond heterolysis of its [H_2O−(tpa)-Fe^{III}−OOH] precursor, was explored by means of hybrid density functional theory. The mechanism for alkane hydroxylation by the high-valent iron–oxo species invoked as an intermediate in Fe(tpa)/H_2O_2 catalysis was investigated. Hydroxylation of methane and propane by HO−Fe^{V}=O was studied by following the rebound mechanism associated with the heme center of cytochrome P450, and it is demonstrated that this species is capable of stereospecific alkane hydroxylation. The mechanism proposed for alkane hydroxylation by HO−Fe^{V}=O accounts for the experimentally observed incorporation of solvent water into the products. An investigation of the possible hydroxylation of acetonitrile (i.e., the solvent used in the experiments) shows that the activation energy for hydrogen-atom abstraction by HO−Fe^{V}=O is rather high and, in fact, rather similar to that of methane, despite the similarity of the H−CH_2CN bond strength to that of the secondary C−H bond in propane. This result indicates that the kinetics of hydrogen-atom abstraction are strongly affected by the cyano group and rationalizes the lack of experimental evidence for solvent hydroxylation in competition with that of substrates such as cyclohexane.

Keywords: density functional calculations · homogeneous catalysis · hydroxylation · iron · O−O activation

Introduction

Mononuclear, non-heme iron enzymes are involved in a wide variety of key biological processes that start with dioxygen activation.[1,2] Intense biochemical investigations have been dedicated to clarifying catalysis by these enzymes, in which the active site hosts an iron complex with a coordination environment dominated by oxygen and nitrogen ligands (i.e., histidine, aspartate, glutamate, tyrosine).[3] Much experimental effort has been devoted to investigation of synthetic complexes aimed at mimicking the chemistry of non-heme iron oxygenases.[1] Biomimetic complexes may not only provide useful insights into the enzymatic activity, but they can also serve as new powerful bio-inspired catalysts.

Interesting catalytic activity has been observed for a family of non-heme iron complexes represented by [Fe^{II}-(tpa)$(CH_3CN)_2]^{2+}$, in which TPA is the tetradentate tripodal tris(2-pyridylmethyl)amine ligand. These catalysts utilize H_2O_2 to carry out stereospecific alkane hydroxylation as well as olefin epoxidation and *cis*-dihydroxylation,[4–6] the last-named being a reaction not previously known to be effected by a synthetic iron complex. Isotopic labeling experiments provide compelling evidence for the probable involvement of a formally iron(v)–oxo species in these oxidations. For example, it has been observed that alkane hydroxylation occurs with complete retention of stereochemistry, but with some incorporation of ^{18}O from added $H_2{}^{18}O$ into the alcohol product.[4] The extent of label incorporation from $H_2{}^{18}O$ depends on the strength of the alkane C−H bond: the stronger the bond, the more oxygen from water is incorporated. These experiments suggest the involvement of a highly selective metal-based oxidant capable of introducing water into the product. It is thus proposed that the active oxidant is a HO−Fe^{V}=O species derived from O−O

[a] Dr. A. Bassan, Prof. M. R. A. Blomberg, Prof. P. E. M. Siegbahn
Department of Physics, SE-10691
Stockholm (Sweden)
Fax: (+46) 8-55378600
E-mail: arianna@physto.se

[b] Prof. L. Que, Jr.
Department of Chemistry and Center for Metals in Biocatalysis
University of Minnesota, Minneapolis, Minnesota 55455 (USA)

Supporting information for this article is available on the WWW under http://www.chemeurj.org/ or from the author: Cartesian coordinates of stationary points and tables with absolute energies.

DOI: 10.1002/chem.200400383

heterolysis of its $[Fe(tpa)(H_2O)(OOH)]^{2+}$ precursor, which is formed from the reaction of $[Fe^{II}(tpa)(CH_3CN)_2]^{2+}$ and H_2O_2 (Scheme 1). The $[Fe(tpa)(OOH)]^{2+}$ species has indeed been characterized and found to have a low-spin ground state.[7,8] The coordination of water as the sixth ligand in the $Fe^{III}(OOH)$ complex provides the mechanism for water incorporation into the proposed $HO-Fe^{V}=O$ oxidant. Isotopic labeling results for olefin oxidation provide strong support for this mechanism. As in Fe(tpa)-catalyzed alkane hydroxylation, there is some incorporation of label from $H_2{}^{18}O$ into the epoxide product. More persuasively, the *cis*-diol product shows the incorporation of one oxygen atom from H_2O_2 and one oxygen atom from H_2O, a result that requires the sole involvement of the $HO-Fe^{V}=O$ moiety having one oxygen atom from water and one oxygen atom from hydrogen peroxide.[5]

This type of high-valent iron–oxo intermediate has been invoked in the catalysis of some non-heme iron enzymes, namely, the Rieske-type dioxygenases, which catalyze *cis*-dihydroxylation of aromatic compounds.[9,10] The proposed mechanism involving a formally iron(v)–oxo species also has similarities to the heme chemistry of cytochrome P450, for which a similar high-valent iron–oxo species, namely, $[(Por^{\bullet})Fe^{IV}=O]^{+}$ is suggested as the key oxidizing intermediate.[11]

Previous theoretical studies have demonstrated the feasibility of O–O bond heterolysis leading to the $HO-Fe^{V}=O$ species.[12] The present study is aimed at gaining mechanistic insight into the steps subsequent to $HO-Fe^{V}=O$ formation, that is, the transformations leading to substrate oxidation. Here we consider specifically the hydroxylations of methane and propane, which occur by slightly different routes that depend on the strength of the C–H bond being cleaved. The hydroxylation of acetonitrile was also studied, since it is the solvent used in the experiments.

Computational Methods

Density functional theory (DFT) was employed to explore how the high-valent iron–oxo species $HO-Fe^{V}=O$ can react with alkanes and acetonitrile. The B3LYP functional,[13] which includes the Becke three-parameter exchange[14] and the Lee, Yang, and Parr correlation functionals,[15] was used.

The energy profiles and the structures included in the present study were obtained by means of the quantum chemical programs Jaguar 4.2[16] and Gaussian 98.[17] Fully optimized transition states were obtained by evaluation of the second derivatives with respect to the nuclear coordinates (Hessian) of approximate transition-state structures. Second derivatives were essential for confirming that the optimized transition state was characterized by only one imaginary frequency corresponding to the normal mode associated with the reaction coordinate. Hessians for reactants, intermediates, and transition states were also needed to derive the zero-point effects and the thermal corrections necessary for determining Gibbs free energies. The thermochemical analysis, which uses standard expressions for an ideal gas in the canonical ensemble, treated the normal modes within the harmonic approximation. The corrections to the Gibbs free energies were computed with respect to a supercluster including both the iron complex and the substrate. Account has be taken of the fact that this type of approach may lead to underestimation of the actual energy barrier because some loss of entropy is neglected.

An effective core potential was used to describe iron.[18] In the geometry optimizations and Hessian evaluations all other atoms were described by a standard double zeta basis set, denoted lacvp in Jaguar. The final B3LYP energies for the fully optimized structures were computed by using a large basis set with polarization functions an all atoms (denoted lacv3p** in Jaguar[16]). In the present work, free energies are reported with inclusion of zero-point and thermal effects, evaluated for a temperature of 298.15 K. Spin populations obtained with the lacvp basis set are reported.

Concerning spin populations and oxidation states, the oxidation state of a mononuclear metal complex does not require careful analysis of the wave function, but in general follows more or less directly from the input specification of total charge on the basis of general conventions. Exceptions might occur where, for example, an expected iron(IV) state instead becomes an iron(III) state with a ligand radical. This situation is easily recognized from the computed spin populations. If an unrealistic oxidation state were to appear for some intermediate in the calculations, this can easily be judged because the energy is too high. Furthermore, for high-spin iron complexes the spin distribution on the metal does not strictly correspond to the number of d electrons expected from the oxidation state. A typical case is iron(III), which in the high-spin state ($S=5/2$) gives rise to a spin population of about 4 on the metal, with the remaining spin density delocalized an the ligands. When an iron–oxo moiety is present, the convention is to assign the oxidation state of iron by considering the oxo ligand to be an oxide anion (O^{2-}), while the spin distributions are more easily interpreted in terms of the electronic configuration associated with the Fe=O double bond, which resembles the electronic configuration of triplet dioxygen.[19,20]

To reproduce the polarization effects of acetonitrile, which is the solvent used in the experiments,[4,5] the self-consistent reaction field as implemented in Jaguar was employed.[21,22] The solvent was modeled as a macroscopic continuum with dielectric constant $\varepsilon=36.64$, and the solute was placed in a cavity contained in this continuous medium. The probe radius used for acetonitrile molecules was 2.155 Å. Final energies of the optimized structures were corrected for the solvent effects by employing the lacvp basis set. As explained below, the investigation of oxo–hydroxo tautomerization, which involves strong hydrogen bonds, required a slightly different procedure to account for the polarization induced by the solvent. In this case, geometry optimizations in solution were necessary.

The accuracy of the B3LYP functional can be ascertained from benchmark tests on a wide array of molecules (radicals, non-hydrogen systems, hydrocarbons, substituted hydrocarbons, and inorganic hydrides)[23–25] and transition-metal systems.[26–30] From the available data, it can be determined that an error of about 3–5 kcal mol^{-1} could affect the energy profiles reported in the present investigation. However, such an accuracy should be sufficient to discriminate among different reaction mechanisms.[31,32] Note that other theoretical studies on TPA complexes[33] and similar systems[34] indicate that the chosen hybrid functional is capable of predicting the proper spin for the ground state. In the present work the performance of B3LYP is compared to a G2MP2 extrapolation scheme for some probe reactions, namely, hydrogen-atom abstraction from propane, methane, and acetonitrile by the hydroperoxyl radical. The optimized geometries obtained from the B3LYP approach described above were used to calculate the energies on the basis of G2MS [Eq. (1)]:[35]

$$E(\mathrm{G2MS}) = E[\mathrm{CCSD(T)/6\text{-}31G(d)}] + \mathrm{E}[\mathrm{MP2/6\text{-}311+G(2df,2p)}] - E[\mathrm{MP2/6\text{-}31G(d)}] \quad (1)$$

The free energy G(G2MS) was then obtained by using the corrections (i.e., solvent, zero-point, and thermal) derived from the B3LYP approach. In one case, the more accurate G2 energies based on the MP4/6-311G(d,p) level were calculated; the expressions for the corrections in the G2 scheme are described in ref. [36].

A case of spin contamination was encountered in the study on the low-spin state for the high-valent iron–oxo species. An approximate correction to the energy was therefore derived from the energies of the low-spin ("broken symmetry") and high-spin states together with the Heisenberg spin Hamiltonian formalism.[37]

Results and Discussion

Experiments on alkane hydroxylation and olefin oxidation with the non-heme Fe(tpa) catalyst suggested a mechanism involving a formally HO–Fe^{V}=O intermediate, formed by O–O heterolysis of its H_2O–Fe^{III}–OOH precursor (Scheme 1).[4–6] Theoretical studies based on DFT have demonstrated the viability of the O–O heterolytic cleavage, which affords the high-valent iron–oxo species. [12] The present theoretical study goes further and investigates the reactivity of HO–Fe^{V}=O toward alkanes. A description of the high-valent iron–oxo species is presented first. Then the reaction mechanism for the hydroxylation of methane and propane is discussed. Finally hydroxylation of acetonitrile is examined, since it is the solvent used in the experiments and its C–H bond strength is comparable to the secondary C–H bond strength of propane (vide infra).

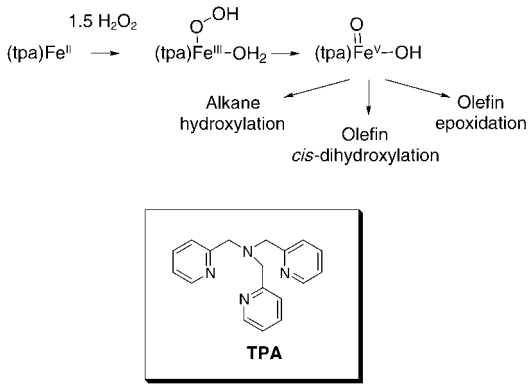

Scheme 1. Proposed mechanism for alkane hydroxylation and olefin oxidation by $[Fe^{II}(tpa)(CH_3CN)_2]^{2+}$ and H_2O_2.

The HO–Fe^{V}(tpa)=O species: Previous theoretical studies demonstrated that a high-valent iron–oxo species can be generated by O–O heterolysis of the $[Fe(tpa)(H_2O)(OOH)]^{2+}$ precursor, in which the presence of a water molecule in the octahedral coordination sphere of the metal complex promotes O–O bond cleavage. [12] The product of the cleavage is the *cis*-HO–Fe^{V}=O species depicted in Figure la, in which the hydroxo ligand and the free water molecule are generated during O–O heterolysis of the peroxo ligand. The ground state for the high-valent iron–oxo species is a quartet ($S=3/2$), which is calculated to have a rather short Fe–O bond (1.66 Å) and a longer Fe–OH bond (1.77 Å). Our calculations show that unpaired spin density is distributed mainly within the HO–Fe^{V}=O unit with spin populations of 1.58 on the Fe atom, 1.00 on the oxo atom, and 0.44 on the hydroxo oxygen atom. This spin distribution is not unlike that found for compounds I of heme peroxidases and cytochrome P450, and related model complexes.[38–40] The iron centers in the high-valent heme complexes are also formally Fe^{V}, but are better described as Fe^{IV}=O coupled to a porphyrin radical cation. The description of the $S=1$ Fe^{IV}=O center is analogous to that in triplet O_2: two unpaired electrons are accommodated in two π* orbitals with spin populations of about 1 on both the metal and the oxo group.[19,20] The unpaired electron on the porphyrin radical then interacts weakly with the $S=1$ Fe^{IV}=O center to afford almost degenerate quartet and doublet states. In the ground state of the biomimetic non-heme iron complex, the third unpaired electron is instead ferromagnetically coupled to the other two unpaired spins and thus lowers the total energy by maximizing the exchange interaction. Although this unpaired electron is mainly localized on

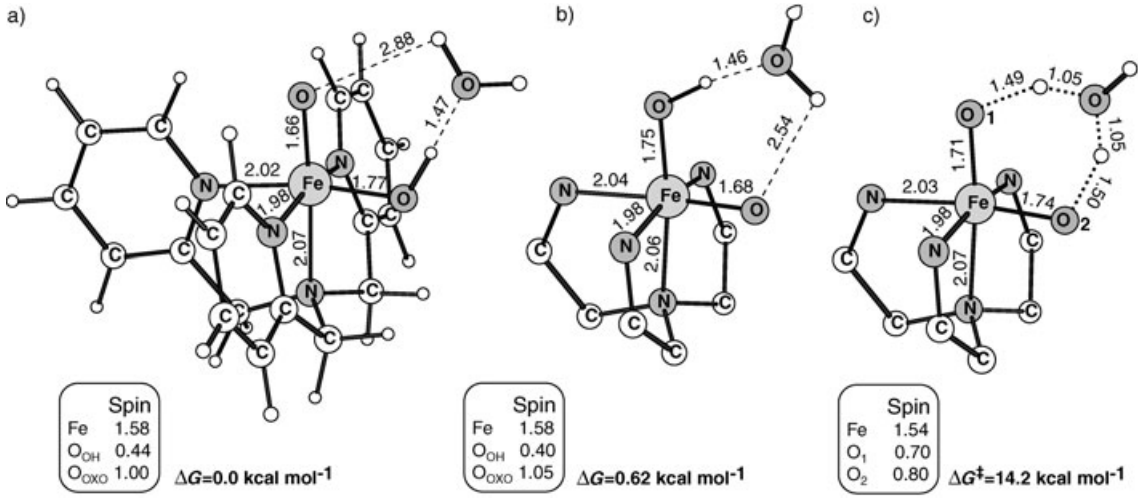

Figure 1. a) The *cis*-HO–Fe^{V}(tpa)=O species in which the oxo group occupies the position *trans* to the amine nitrogen atom. b) The *cis*-HO–Fe^{V}(tpa)=O species in which the oxo group occupies the position *trans* to one of the aromatic nitrogen atoms (for clarity only part of the TPA ligand is depicted). c) Transition state for oxo–hydroxo tautomerization mediated by a water molecule. Bond lengths in Å are shown together with the corresponding spin densities and relative energies.

iron, some spin density is delocalized on the hydroxo ligand, owing to transfer of spin density from the hydroxo ligand to the metal atom. The electronic structure of the HO−Fe^{V}=O species can thus be described by two extremes: in one resonance form the metal center has oxidation state five with three unpaired electrons on the Fe=O moiety. The other resonance form consists of the metal center with oxidation state four ($S=1$) and the OH ligand with a hole, which is ferromagnetically coupled to attain the $S=3/2$ state. There are ample precedents for oxoiron(IV) moieties with $S=1$ states in biological and biomimetic heme centers[41–43] and, more recently, in synthetic non-heme iron complexes as well, including $[Fe^{IV}(O)(tpa)]^{2+}$.[44–46]

Two tautomers are possible for the *cis*-HO−Fe^{V}=O species: as illustrated in Figure la the oxo group can occupy the position *trans* to the sp^3 amine nitrogen or *trans* to one of the aromatic nitrogen atoms (Figure lb). The two complexes, which have very similar structural parameters and spin densities, differ by less than 1 kcal mol^{-1} in energy and can be considered as almost degenerate. Conversion between the two structures may be mediated by the hydrogen-bonding water molecule, which serves as a proton shuttle. A highly symmetric transition state for the oxo–hydroxo tautomerization involving the water molecule was located; the geometrical details and spin populations for this transition state are reported in Figure lc. A barrier of 14.2 kcal mol^{-1} was obtained for oxo–hydroxo tautomerization.

The tautomerization was also investigated by using a different model, in which a molecule of acetonitrile (i.e., the solvent) forms a hydrogen bond with water (Figure 2a). In this way the transition state, which involves the H_3O^+ ion, should be stabilized by the hydrogen-bonding solvent. Introduction of polarization effects of the medium proved to be essential for locating the minima, and therefore the tautomerization with the model depicted in Figure 2a was investigated by optimizing geometries in solution (see Computational Methods). With this type of computational approach only an approximate transition state was located (Figure 2b), for which the thermal effects of the Gibbs free energy could not be evaluated. The structures of the *cis*-HO−Fe^{IV}=O species and the transition state obtained with the small model (Figure la and c) are rather similar to the corresponding strucatures obtained with the larger model (Figure 2a and b). However, the presence of acetonitrile with a hydrogen bond to the water molecule significantly lowers the barrier for oxo–hydroxo tautomerization. The computed activation energy for the large model, corrected for thermal effects from the small model, is 10.5 kcal mol^{-1}. Since O−O heterolysis was found to be endergonic by 5.1 kcal mol^{-1} with respect to the $[Fe(tpa)(OOH)]^{2+}$ reactant,[12] it can be concluded that the tautomerization reaction involves a total barrier of 15.6 kcal mol^{-1}.

Alkane hydroxylation: The reactivity of HO−Fe^{V}=O toward alkanes was studied by exploring the hydroxylation of methane and propane. In the case of propane, formation of 2-propanol was investigated. Since the hydrogen-bonding

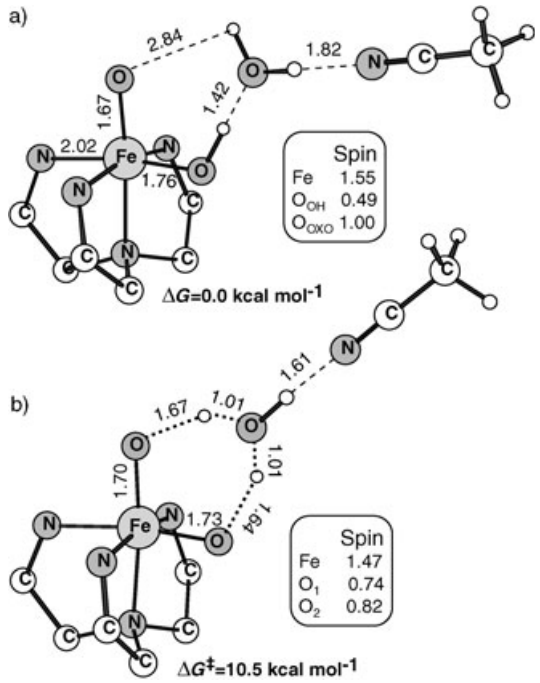

Figure 2. The model used to account for the strong polarization effects of the solvent (i.e., acetonitrile) in oxo–hydroxo tautomerization. The structures of a) HO−Fe^{V}(tpa)=O and b) the approximate transition state were obtained by means of geometry optimizations in solution. Bond lengths in Å are shown together with the corresponding spin densities; for clarity only part of the TPA ligand is depicted.

water molecule of Figure 1 is not involved in the reaction pathway leading to the hydroxylated products, the model for the present investigation does not contain water in the second coordination shell of the metal complex. Furthermore, the reactivity of the slightly more stable tautomer with the oxo group in the position *trans* to the amine nitrogen atom (Figure la) is discussed; it has been verified that the two tautomers behave very similarly. The reactive species (**M-reac**) is thus the cluster of Figure 3, in which the alkane is located in the second coordination sphere of the HO−Fe^{V}=O complex. The electronic structure and geometry of HO−Fe^{V}=O is not significantly perturbed by the presence of the substrate as compared to the HO−Fe^{V}=O species of Figure la. There are, however, some differences for some of the bond lengths and for the computed spin densities. These differences can be attributed mainly to the loss of the rather strong hydrogen bond between the hydroxo ligand and the water molecule.

The mechanism for alkane hydroxylation was explored by following the rebound paradigm, which first involves abstraction of a hydrogen atom from the alkane to give an alkyl radical (Scheme 2).[47,48] Subsequently, the radical rebound step gives the final hydroxylated product and a complex in which the metal center has changed its oxidation state from Fe^{V} to Fe^{III}. Because the chemical transformations described below involve different spin states of the iron complex, it is important to note that for HO−Fe^{V}=O

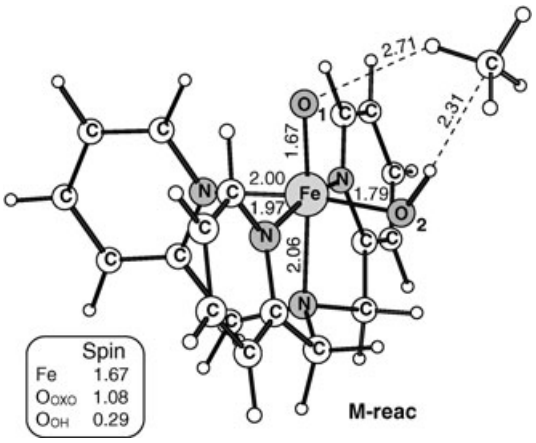

Figure 3. The reactant in methane hydroxylation, in which the alkane is located in the second coordination shell of the metal complex. Spin densities and bond lengths in Å are shown.

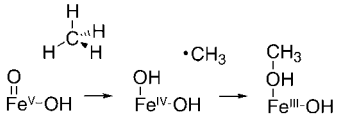

Scheme 2. The rebound mechanism in alkane hydroxylation by HO–Fe^{V}=O.

two states other than the quartet ground state are possible: the doublet ($S=1/2$) and the sextet ($S=5/2$). As shown in Table 1, which reports the most important structural parameters and the spin distributions for the three spin states, the sextet and the doublet states are more than 10 kcal mol^{-1} higher in energy than the quartet ground state.

Table 1. Comparison of geometrical parameters and spin densities of the three possible spin states for HO–Fe^{V}=O: doublet ($S=1/2$), quartet ($S=3/2$), and sextet ($S=5/2$). Relative energies are also reported. O1 refers to the oxo group, and O2 to the oxygen atom of the hydroxo ligand (see Figure 3).

	d(Fe–O1) [Å]	d(Fe–O2H) [Å]	Spin(Fe)	Spin(O1)	Spin(O2)	ΔE [kcal mol^{-1}]
doublet	1.74	1.77	1.58	−0.80	0.30	12.4+6.4 (18.8)[a]
doublet′	1.68	1.80	0.21	1.25	−0.48	13.7+6.8 (20.5)[a]
quartet	1.67	1.79	1.67	1.08	0.29	0.0
sextet	1.72	1.86	2.97	1.01	0.71	17.4

[a] For the quartet and the sextet states, the $\langle S^2\rangle$ expectation values (3.78 and 8.80, respectively) indicate a low level of spin contamination; for the doublet states the spin contamination (the $\langle S^2\rangle$ expectation values are 1.79 and 1.77) affects the relative energies, whose corrections of 6.4 and 6.8 kcal mol^{-1} were estimated from the Heisenberg spin Hamiltonian formalism.[37]

Two electronic configurations arise when $S=1/2$, and they can be interpreted in terms of the two possible couplings of the three unpaired electrons characterizing the ground state ($S=3/2$) of the iron–oxo moiety. Either the two π* electrons are antiferromagnetically coupled, or alternatively the unpaired d electron can be antiferromagnetically coupled to the two π* electrons. Although the two doublet states of HO–Fe^{V}=O have different electronic configurations, they are found to differ by only 1.3 kcal mol^{-1}, lying at +12.4 and +13.7 kcal mol^{-1} with respect to the quartet ground state. As a comparison, for cytochrome P450 the doublet state, which is almost degenerate with the quartet state, has the two unpaired π* electrons antiferromagnetically coupled to an unpaired electron localized an the porphyrin ligand, giving a total spin of $S=1/2$.

While the $\langle S^2\rangle$ expectation values for the quartet and the sextet states indicate negligible spin contamination, the doublet states are heavily contaminated by higher spin states. As explained in the section on Computational Methods, approximate corrections to the energies of the two states with a high-level of spin contamination were estimated from the Heisenberg spin Hamiltonian formalism. Corrections of about 6.4 and 6.8 kcal mol^{-1} were obtained (see Table 1), which destabilize the doublet states even more with respect to the quartet ground state.

Methane hydroxylation: The three potential-energy surfaces ($S=1/2$, 3/2, 5/2), which are quite different in energy on the reactant side, become energetically very similar along the reaction pathway leading to the hydroxylated alkane. For methane hydroxylation the energy profiles of the rebound mechanism along the doublet and the quartet potential-energy surfaces are illustrated in Figure 4. When the quartet state is considered, the first step of the hydroxylation passes through the transition state **M-tsab** (Figure 5a), in which one hydrogen atom of methane is abstracted by the oxo group of the metal complex. During this transformation a radical develops on the substrate, as indicated by the spin density of 0.68 computed on methane in the transition state (Figure 5a). The hydrogen-atom abstraction implies reduction of the metal from iron(v) to iron(iv) and the formation of a new OH ligand. The transition state of Figure 5a decays to an intermediate in which iron is coordinated by two hydroxo ligands, and the methyl radical is located in the second coordination shell of the metal complex (**M-Fe^{IV}**). The structural details and the spin distribution computed for this intermediate are reported in Figure 5b. The spin density of iron has not changed significantly with respect to that obtained for the HO–Fe^{V}=O species: the spin densities are 1.67 in the reactant and 1.66 in the iron(iv)–hydroxo intermediate. So the formation of the methyl radical (spin population at C1: 1.04) occurs concomitantly with the loss of unpaired spin density at the terminal oxo and hydroxo ligands of the oxidant. While the computed spin population of 1.67 in the reactant can be interpreted in terms of the electronic

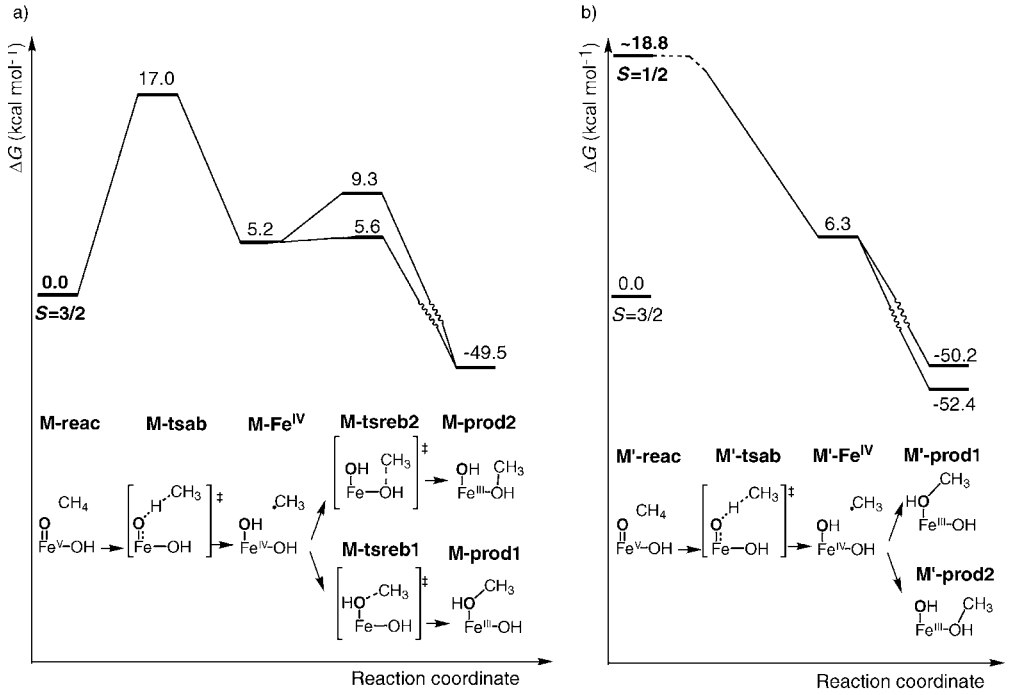

Figure 4. Energy profiles for the rebound mechanism of methane hydroxylation along the quartet potential-energy surface ($S=3/2$; a) and the doublet potential-energy surface ($S=1/2$; b). Free energies in kcal mol^{-1} are reported.

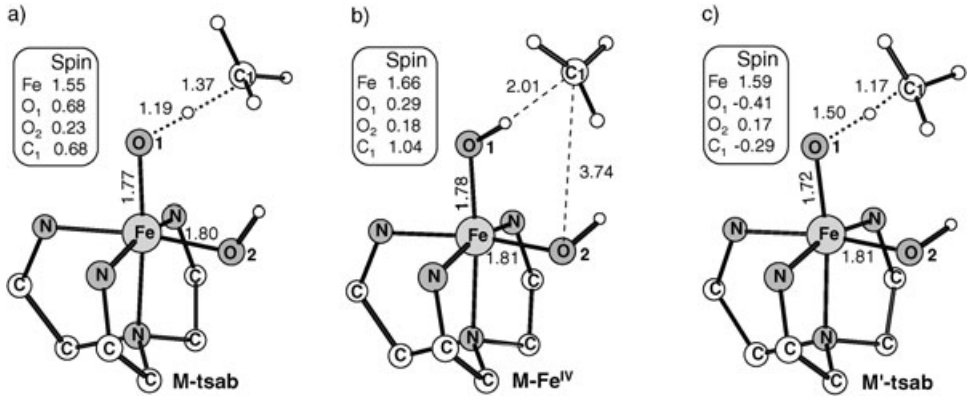

Figure 5. a) Transition state for hydrogen-atom abstraction in methane hydroxylation along the quartet potential-energy surface ($S=3/2$). b) The iron(IV)–hydroxo intermediate formed by hydrogen-atom abstraction ($S=3/2$). c) Transition state for hydrogen-atom abstraction in methane hydroxylation along the doublet potential-energy surface ($S=1/2$). Bond lengths in Å and spin densities are shown. For clarity the TPA ligand is only partially depicted.

The energy diagram in Figure 4a shows that the computed barrier for hydrogen-atom abstraction is 17.0 kcal mol^{-1}. Zero-point effects lower the barrier by 4.2 kcal mol^{-1}, while thermal effects, in particular the entropy contribution, increase it by 3.3 kcal mol^{-1}. With respect to the HO–Fe^{V}=O species, hydrogen-atom abstraction occurs with an endergonicity of 5.2 kcal mol^{-1}.

The iron(IV)–hydroxo intermediate of Figure 5b is almost degenerate with the corresponding doublet structure, in which the unpaired electron on the methyl group is antiferromagnetically coupled with the two unpaired d electrons of iron. Because of the weak coupling between the unpaired d electrons and the unpaired electron of the substrate, the doublet species is only 1.1 kcal mol^{-1} higher in energy than the corresponding quartet, as illustrated in the energy diagrams of Figure 4 (because of the small energy difference, effects of spin contamination were neglected in this case). The doublet state of the iron(IV)–hydroxo intermediate can be formed by hydrogen-atom abstraction along the doublet surface via transition state **M′-tsab** (Figure 5c). Because of the broken-symmetry structure associated with the short Fe=O double bond, the new spin density of 1.66 reflects the intermediate spin state ($S=1$) of iron(IV) in an octahedral environment, which yields two unpaired d electrons on iron. As usual some spin density is delocalized on the ligands and in particular on the two OH groups. The rearrangement of the electronic structure during hydrogen-atom abstraction also explains the lengthening of the Fe–O bond length from 1.67 Å in the Fe^{V}=O species to 1.78 Å in the iron(IV)–hydroxo species of Figure 5b.

correction in the reactant, the energy barrier associated with the $S=1/2$ hydrogen-atom abstraction step disappears. A comparison between **M′-tsab** of Figure 5c and the corresponding transition state on the quartet surface (Figures 5c and a) shows that the transition state with $S=1/2$ resembles the reactant structure (i.e., hydrogen-atom abstraction has proceeded only to a small extent), while the transition state with $S=3/2$ is more similar to the iron(IV)–hydroxo intermediate. It is difficult to derive the exact activation energy associated with hydrogen-atom abstraction when $S=1/2$ due to the high degree of spin contamination. However, the doublet potential-energy surface does not involve reaction pathways lower than the quartet one. Low-energy pathways could not be located on the sextet potential-energy surface either. For example, the sextet iron(IV)–hydroxo intermediate is found to lie 5.8 kcal mol^{-1} above the corresponding quartet state **M-Fe^{IV}**.

After hydrogen-atom abstraction, the methyl radical combines with one of the OH groups in the subsequent rebound step to generate the final product. Two different pathways are possible at this stage of the reaction. The methyl radical can recombine with the hydroxo ligand originating from the oxo group (O1), or the rebound process can involve O2 of the other OH ligand (see labeling in Figure 5b). Both these chemical transformations involve activation energies that are lower than the barriers obtained for hydrogen-atom abstraction. When the rebound step on the quartet potential-energy surface is considered, the recombination with O1 passes through transition state **M-tsreb1**, which is 5.6 kcal mol^{-1} higher in energy than the reactant HO–Fe^{V}=O species. The recombination of the methyl radical with O2 involves a barrier of 9.3 kcal mol^{-1} (**M-tsreb2** in Figure 4a). The different activation energies obtained for the two possible recombinations originate from solvent corrections added to the free energies (see Computational Methods). While the rebound step involving O1 is favored by the presence of the solvent, the solvent corrections increase the activation energy for the rebound step involving O2.

Although different in energy, the two transition states have rather similar structural parameters, as shown in Figures 6a and b, in which the most important distances are highlighted together with spin populations. The two transition states are characterized by a rather long distance (2.8–2.9 Å) between the methyl carbon and oxygen atoms. They decay to two different products: the Fe^{III} complex in which bound methanol occupies the position *trans* to the amine nitrogen atom, and that in which it is situated *trans* to one of the aromatic nitrogen atoms. As shown in the energy diagram of Figure 4, the hydroxylation reaction along the quartet surface is exergonic by 49.5 kcal mol^{-1} for both products.

When the doublet potential-energy surface is explored, it is estimated that the recombinations with O1 or with O2 have almost zero barriers with respect to the iron(IV)–hydroxo intermediate. It follows that hydrogen-atom abstraction and the rebound step along the doublet surface may be considered to occur in a concerted fashion. The fast rebound step results from the favorable coupling between the singly

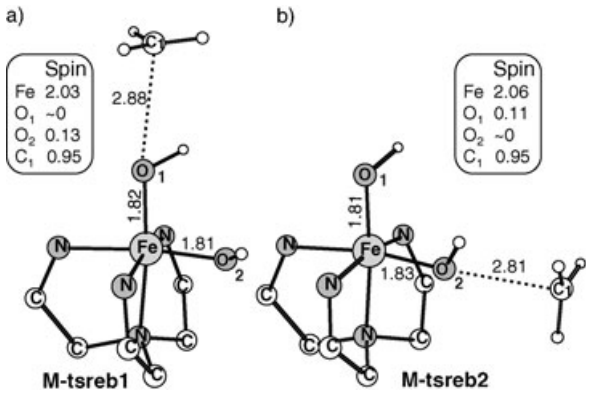

Figure 6. a) Transition state for recombination ($S=3/2$) of the methyl radical with the oxygen atom (O1) *trans* to the amine nitrogen atom. b) Transition state for recombination ($S=3/2$) of the methyl radical with the oxygen atom (O2) *trans* to one of the aromatic nitrogen atoms. The spin populations of the metal complex and of the substrate are shown together with bond lengths in Å. For clarity the TPA ligand is only partially depicted.

occupied methyl orbital and the unpaired electrons of the iron(IV)–hydroxo species. In the doublet state of the iron(IV)–hydroxo intermediate two unpaired electrons occupy the d orbitals of iron, and they are antiferromagnetically coupled with the unpaired electron located on the methyl radical. During the formation of the C–O bond in the rebound step (see Figure 6), one electron is donated to iron, which changes its oxidation state from four to three.[40,47]. The β-electron of the methyl radical thus has the proper spin to complete the double occupation of one of the d orbitals. The electron transfer associated with C–O bond formation leads to the low-spin Fe^{III} product with $S=1/2$. In the quartet state, the unpaired electron of the methyl radical is ferromagnetically coupled with the two d electrons on iron. This α-electron is then donated to an empty d orbital during C–O bond formation leading to the quartet Fe^{III} product, which is characterized by three unpaired electrons on the metal center.

Figure 7 summarizes relative energies, structural parameters, and spin distributions for the two possible products (**M-prod1**, **M-prod2**) in their corresponding quartet and doublet states. The ground state of the product is neither the doublet nor the quartet; it is the sextet Fe^{III} complex ($S=5/2$).[49] Still, the rebound step for $S=5/2$ is estimated to involve a barrier which is higher than those for $S=1/2$ and $S=3/2$, and therefore the reaction along the sextet potential-energy surface was not investigated in detail. Figure 7 also shows that the doublet Fe^{III} complex is more stable than the corresponding quartet structure. Because of the shapes of the potential-energy surfaces, spin crossing from the quartet to the doublet or sextet states is expected at a late stage of the hydroxylation reaction. Exactly where the crossing occurs could not be determined.

The product in which methanol occupies the position *trans* to one of the aromatic nitrogen atoms (**M-prod2**) is in general favored over the other product (**M-prod1**), especially in the doublet and sextet cases, because the stronger hy-

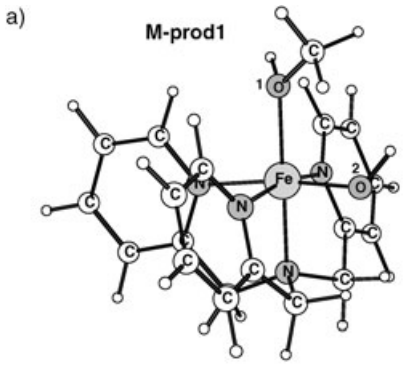

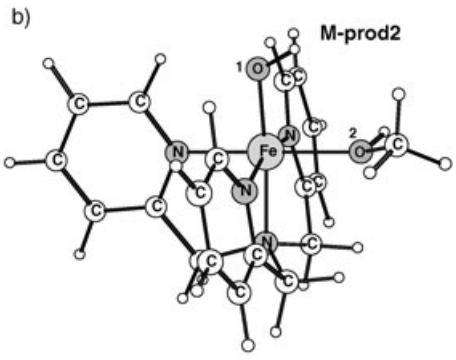

	d(FeO$_1$) Å	d(FeO$_2$) Å	α(FeO$_2$H)
Doublet	2.04	1.81	117.0°
Quartet	2.22	1.80	118.7°
Sextet	2.11	1.79	176.9°

	s(Fe)	s(O$_1$)	s(O$_2$)	ΔE kcal mol^{-1}
Doublet	0.89	-	0.17	**8.4**
Quartet	2.77	-	0.11	**9.1**
Sextet	4.02	-	0.46	**4.4**

	d(FeO$_1$) Å	d(FeO$_2$) Å	α(FeO$_1$H)
Doublet	1.81	2.06	117.7°
Quartet	1.80	2.17	116.7°
Sextet	1.79	2.19	171.9°

	s(Fe)	s(O$_1$)	s(O$_2$)	ΔE kcal mol^{-1}
Doublet	0.88	0.17	-	**6.2**
Quartet	2.77	0.05	-	**9.1**
Sextet	4.03	0.44	-	**0.0**

Figure 7. The two products of methane hydroxylation by HO–Fe^{V}=O. Some relevant structural details such as Fe–O distances (d) and Fe-O-H angles (α) are reported for the three possible spin states (S=1/2, 3/2, 5/2). Spin densities and relative energies are also given.

droxo ligand (relative to methanol) is located *trans* to the weaker amine nitrogen atom (relative to pyridine). Interestingly, opposite entropy and solvent effects are obtained for the different spin states of the two products. The entropy gives rise to a larger energy difference between the high-spin states and the low-spin states,[50] in contrast to the solvent effects, which stabilize the low-spin states with respect to the high-spin states.

The energy diagrams of Figure 4 show that the hydrogen-atom abstraction step, which passes over a barrier of 17 kcal mol^{-1}, is rate-determining for methane hydroxylation by the HO–Fe^{V}=O species. Since formation of the high-valent iron–oxo complex was computed to be endergonic by 5.1 kcal mol^{-1}, a final activation energy of about 22 kcal mol^{-1} is obtained.

The computed pathways for the biomimetic, non-heme, high-valent, iron–oxo species show some resemblance to those of the widely studied compound I of heme enzymes. The energy profiles for the rebound mechanism with the TPA catalyst (Figure 4) can be compared to those for cytochrome P450 proposed by Shaik et al.[40,47] Interestingly, hydrogen-atom abstraction leads to the iron(IV)–hydroxo intermediate in the TPA catalyst, while an iron(III)–hydroxo species is instead formed in cytochrome P450; however, a radical on the porphyrin ligand is also present ([(Por•)Fe^{III}OH]$^{+}$). The recombination step is thus associated with electron transfer to the porphyrin in the case of P450, while the electron is transfered to the metal in the rebound step of the Fe(tpa) system. As in the case of cytochrome P450, for which the high- and low-spin states have been suggested to play a key role in the reactivity of compound I (two-state reactivity),[40] the rebound mechanism for the HO–Fe^{V}=O species in Fe(tpa) may also involve the quartet and doublet potential-energy surfaces (Figure 4). In both systems, the doublet surfaces support a concerted mechanism, while the quartet surfaces favor a stepwise mechanism. However, it is important to point out that the two states are almost degenerate for [(Por•)-Fe^{IV}O]$^{+}$, while they differ by more than 10 kcal mol^{-1} in the HO–Fe^{V}=O species.

Propane hydroxylation: A lower barrier for propane hydroxylation is found due to the weaker secondary C–H bond. The reaction mechanism of propane hydroxylation again starts with hydrogen-atom abstraction by the oxo group. This step involves transition state **P-tsab** (Figure 8), which lies 7 kcal mol^{-1} higher in energy than the HO–Fe^{V}=O reactant. Similarly to hydrogen-atom abstraction in methane hydroxylation, a radical starts to develop on propane in the transition state, as indicated by the computed spin populations in Figure 8b. However, the transition state does not decay to a radical intermediate, but instead leads directly to the hydroxylated product, in which propanol is located in the first coordination shell of the metal complex (Figure 9). In contrast to the methane case, in which the methyl radical could be optimized in the presence of the high-valent iron–oxo intermediate (**M-Fe^{IV}** in Figure 5b), the hydrogen-atom abstraction step for propane does not

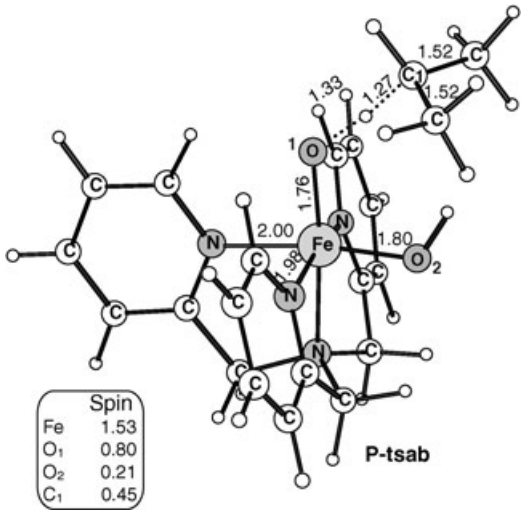

Figure 8. Transition state for hydrogen-atom abstraction from propane along the quartet potential-energy surface (S=3/2). Relevant bond lengths in Å and spin densities are reported.

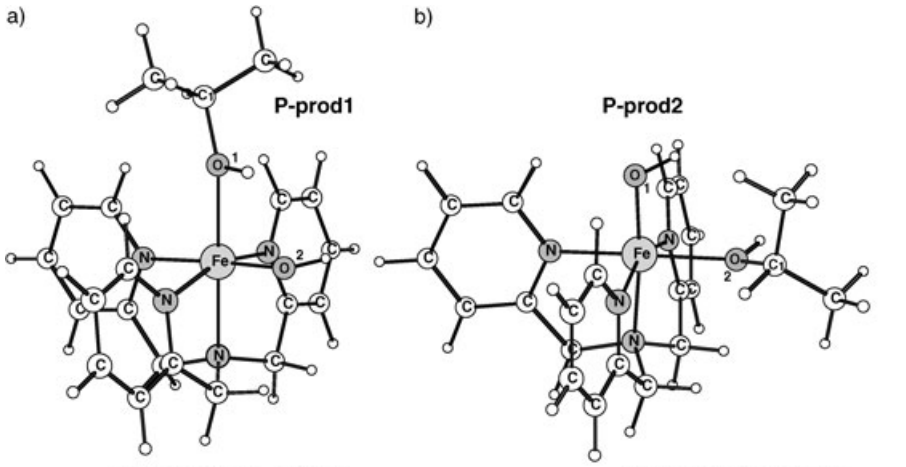

	d(FeO1) Å	d(FeO2) Å	α(FeO2H)
Doublet	2.07	1.82	116.6°
Quartet	2.22	1.81	119.0°
Sextet	2.12	1.80	174.8°

	s(Fe)	s(O1)	s(O2)	ΔE kcal mol-1
Doublet	0.90	-	0.16	**11.8**
Quartet	2.79	-	0.12	**12.6**
Sextet	4.02	-	0.43	**7.1**

	d(FeO1) Å	d(FeO2) Å	α(FeO1H)
Doublet	1.81	2.05	116.6°
Quartet	1.80	2.15	116.3°
Sextet	1.79	2.18	166.8°

	s(Fe)	s(O1)	s(O2)	ΔE kcal mol-1
Doublet	0.90	0.16	-	**7.7**
Quartet	2.78	0.05	-	**11.1**
Sextet	4.04	0.43	-	**0.0**

Figure 9. The two products of propane hydroxylation by HO–Fe^{IV}=O. Some relevant structural details are reported for the three possible spin states ($S=1/2$, 3/2, 5/2). Spin densities and relative energies are also shown.

give any propyl radical and iron(IV)–hydroxo complex. The nascent propyl radical immediately reacts with the nascent iron(IV)–hydroxo species by forming a new C–O bond and thus propanol. This difference may initially appear counterintuitive, since the primary methyl radical would be expected to be more reactive than the secondary isopropyl radical. However, this counterintuitive behavior could be rationalized in terms of the ionization potentials of the alkyl radicals, as discussed previously for MMO.[51] In this argument, formation of the C–O bond implies that an electron is donated by the alkyl radical to the metal center,[40,47] which is reduced to Fe^{III}. The different behaviors of the two alkanes can be understood in terms of the computed lower ionization potential of the propyl radical (170 kcal mol^{-1}) versus the methyl radical (227 kcal mol^{-1}), which thereby drives the transition state of Figure 8 directly toward the formation of propanol. The low ionization potential favors electron transfer to the metal complex and thus the immediate formation of the hydroxylated species without the involvement of a radical species.

The calculations show that the transition-state structure of Figure 8 ($S=3/2$) directly yields product **P-prod1** of Figure 9a, in which propanol results from the rebound of the nascent propyl radical with the oxygen atom O1 coming from the oxo group, which is derived from the oxidant (i.e., H_2O_2). Formation of propanol incorporating not only O1 but also O2 (i.e., the oxygen atom of the OH group originating from water) can occur for the doublet state. When the $S=1/2$ potential-energy surface is examined, it is found that hydrogen-atom abstraction by doublet HO–Fe^{V}=O does not involve any significant barrier. The potential-energy surface around the approximate transition state is rather flat, and the nascent propyl radical can rebind without significant energy barriers with either one of the two OH groups, most likely giving without selectivity either of the two complexes of Figure 9 (**P-prod1** and **P-prod2**). Exploration of the potential-energy surface indicated that electron transfer associated with the hydrogen-atom abstraction (see Scheme 2) occurs at an early stage of the process. This observation may explain why recombination with O2 (i.e., the OH ligand of HO–Fe^{V}=O) is possible along the doublet potential-energy surface: the orientation of propane is still favorable for interaction of the nascent propyl radical with O2 of the OH group. This means that a pathway leading to propanol exists on the doublet potential-energy surface, and it implies a spin transition of the quartet iron(V)–oxohydroxo species to the doublet state, followed by hydrogen-atom abstraction to give propanol. However, the doublet state of the HO–Fe^{V}=O reactant is estimated to lie rather high in energy (see Table 1), and the transformations involving the quartet spin state are thus more probable. Interestingly, calculations also indicate that in the vicinity of the transition state with $S=3/2$ (Figure 8), a spin crossing connects the doublet and the quartet potential-energy surfaces as sketched in the energy diagram of Figure 10. The exact position of the spin crossing could not be located.

Similarly to the methane case, propane hydroxylation is highly exergonic, as indicated in the energy profile of Figure 10, which shows the free energy changes leading to the two products **P-prod1** and **P-prod2**. As summarized in Figure 9, the species in which propanol occupies the position *trans* to one of the aromatic nitrogen atoms (**P-prod2** of Figure 9) is always more stable than the other complex. Among the three possible spin states ($S=1/2$, 3/2, 5/2), the sextet state is always more stable than the doublet and quartet states. As noted above for methanol, entropy effects stabilize the high-spin states,[50] while solvent effects favor the low-spin states.

In summary, according to the energy profiles of Figure 10 the iron(III)–propanol species of Figure 9a can be formed along the quartet or doublet potential-energy surfaces, where finally a spin transition brings the metal complex to the more stable sextet state. The other tautomer (Figure 9b) can instead be formed with $S=1/2$ and then decay to the

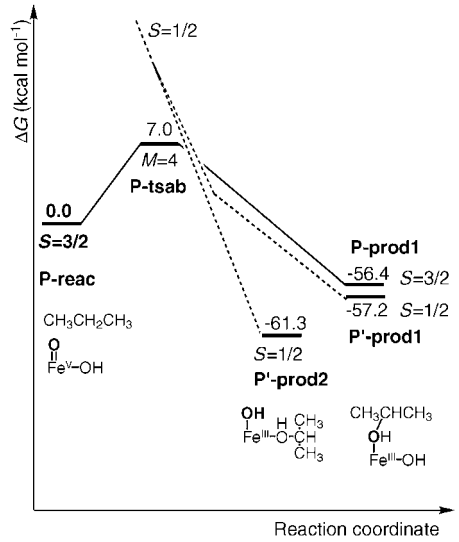

Figure 10. Energy diagram for propane hydroxylation by HO–Fe^{V}=O. Solid line: $S=3/2$ (quartet), dotted line: $S=1/2$ (doublet). **P′-prod1** and **P′-prod2** correspond to the doublet state of the TPA complex.

more stable sextet state. The HO–Fe^{V}=O species is thus capable of hydroxylating secondary alkanes with sufficiently low barriers. In the previous theoretical study, the formation of the high-valent iron–oxo species was computed to be endergonic by 5.1 kcal mol^{-1}.[12] When this value is added to the calculated activation energy of 7 kcal mol^{-1}, a final barrier of only 12.1 kcal mol^{-1} for propanol formation by HO–Fe^{V}=O is obtained.

Hydrogen-atom abstraction—C–H bond strength versus activation energy: The computed energy profiles for methane and propane hydroxylation (Figures 4 and 10) show that hydrogen-atom abstraction requires a higher activation energy for methane than for the weaker secondary C–H bond of propane. For hydroxylation of the primary C–H bond of propane, hydrogen-atom abstraction has a barrier which is about 4 kcal mol^{-1} higher than that of the secondary C–H bond but still lower than that of methane. This result agrees with the bond dissociation energies of the primary C–H bond in propane, which is computed to be 97.1 kcal mol^{-1} and compared to the other two bond dissociation energies in Table 2. Since it is clear that for alkanes the C–H bond strength alone drives the abstraction step by the iron(v)–oxo species, it might be expected that acetonitrile (i.e., the solvent used in the experiments) should also be hydroxylated by the biomimetic species, because the C–H bond strength of acetonitrile is in fact very similar to the computed bond dissociation energy (BDE) of the secondary C–H bond of propane (Table 2). However, such a reaction has not been experimentally observed. To shed light on the possible interaction between the iron(v)–oxo intermediate and the solvent, the rebound mechanism was probed with acetonitrile as substrate. A slightly larger model than was employed for propane and methane had to be used, since acetonitrile

Table 2. Computed bond dissociation energies (BDE) of methane, propane (secondary CH bond), and acetonitrile. Activation and reaction energies corresponding to hydrogen-atom abstraction by HO–Fe^{V}=O are reported.

	CH_4	$H_3CCH_2CH_3$	H_3CCN
BDE[a] [kcal mol^{-1}]	101.6	92.7	92.4
$\Delta G^{\neq}$ [kcal mol^{-1}]	17.0	7.0	18.3
ΔG [kcal mol^{-1}]	5.2	–	−2.5

[a] BDEs are corrected for solvent effects ($\varepsilon=36.64$).

tends to form a hydrogen bond with the hydroxo group of HO–Fe^{V}=O. Two molecules of CH_3CN were therefore included in the model: one representing the substrate and one forming a hydrogen bond to the hydroxo ligand of HO–Fe^{V}=O. This type of model prevents the hydrogen bond between the substrate and the oxidant from affecting the energetics of the rebound process. Hence, the computed activation energies for the hydrogen-atom abstraction and for the rebound step can be directly compared to the corresponding energies of the other two substrates investigated in the present work.

Although the C–H bond strengths of propane and acetonitrile are very similar, the computed activation energies for hydrogen-atom abstraction by the oxo group differ by more than 10 kcal mol^{-1}: the computed energy barriers are 7.0 kcal mol^{-} for propane and 18.3 kcal mol^{-1} for acetonitrile (Table 2). The transition state associated with hydrogen-atom abstraction from CH_3CN ($S=3/2$) is shown in Figure 11 with relevant bond lengths and spin populations. This structure subsequently decays to a stable radical in which the electron is delocalized over the cyano group, as already inferred from the computed spin population of the transition state. The computed energetics for the entire rebound process are displayed in Figure 12.

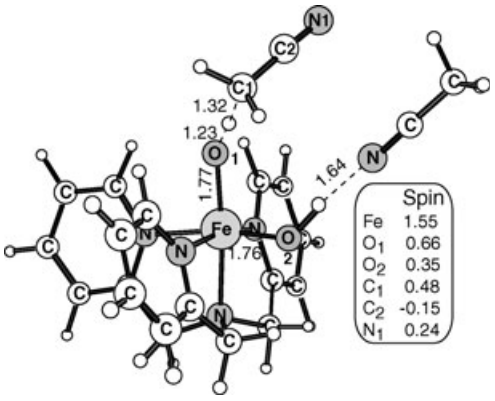

Figure 11. Transition state for hydrogen-atom abstraction from acetonitrile ($S=3/2$). Relevant bond lengths in Å and spin densities are reported.

Hydrogen-atom abstraction from CH_3CN requires an activation energy comparable to that obtained for methane. Also, the C–H and O–H bond lengths of the transition state shown in Figure 11 resemble the corresponding ones of

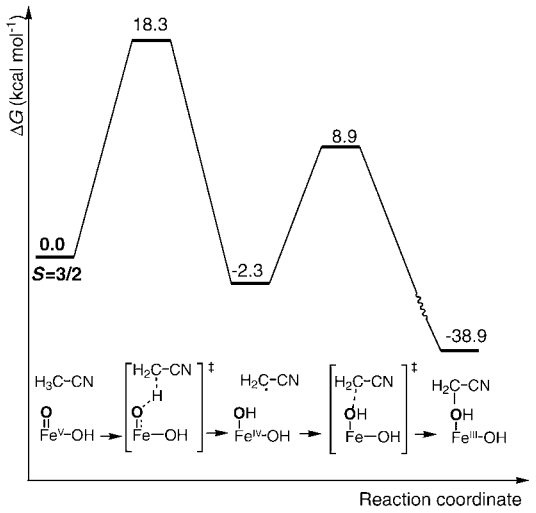

Figure 12. Energy diagram for acetonitrile hydroxylation by $HO-Fe^{V}=O$ ($S=3/2$).

methane (Figure 5) rather than those of propane (Figure 8). However, the energy change of the hydrogen-atom abstraction step yielding the iron(IV)–hydroxo species and a radical on the substrate parallels the C–H BDE, as derived from the computed energies gathered in Table 2. A comparison with the propyl radical cannot be made, since the corresponding intermediate following hydrogen-atom abstraction from propane is not stable and evolves directly to the hydroxylated product. The calculations show that, while the activation energy of hydrogen-atom abstraction from alkanes correlate with the corresponding C–H bond strength, the energy barrier of the same step with acetonitrile as substrate does not depend entirely on the C–H bond strength, but is strongly affected by the presence of the cyano group.

The three substrates, methane, propane, and acetonitrile, give rise to an equivalent energy pattern when a simpler hydrogen-atom abstraction reaction is explored. More specifically, abstraction by the hydroperoxyl radical was investigated, and the corresponding energetics are summarized in Figure 13. Again, the activation energy for hydrogen-atom

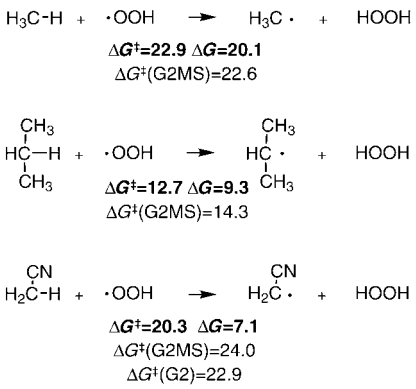

Figure 13. Energetics for a probe hydrogen-atom abstraction step with three different substrates. B3LYP (bold) and G2MS activation energies in kcal mol^{-1} are compared.

abstraction from acetonitrile is more similar to that of methane than that for propane. On the other hand, the free energy changes of the reaction match the trend of the computed C–H BDEs of the three substrates. The computed energy difference for acetonitrile is somewhat lower than that of propane because the products (i.e., the radical and hydrogen peroxide) are characterized by a new hydrogen bond between the cyano group and H_2O_2.

This small model system was used to compare the performance of B3LYP with the G2MS extrapolation scheme in deriving the activation energies for hydrogen-atom abstraction from methane, propane, and acetonitrile (see Computational Methods).[35] These calculations confirm the B3LYP energy pattern and showed again that the energy barrier for hydrogen-atom abstraction for CH_3CN is comparable to that for CH_4. Because the difference between the two methods is somewhat larger for acetonitrile (Figure 13), the more accurate G2 calculation was performed for this substrate;[36] it yielded an activation energy of 22.9 kcal mol^{-1}, which compares to 20.3 kcal mol^{-1} obtained with the B3LYP method. Therefore, the activation barriers for hydrogen-atom abstraction are rather well reproduced (within the expected accuracy) by the B3LYP functional, as was already found in other studies on similar systems.[52,53] This simple reaction corroborates the conclusions obtained from the study on the hydrogen-atom abstraction by the high-valent iron–oxo species, which showed that the thermodynamic and kinetic profiles of hydrogen-atom abstraction for methane and propane correlate with the corresponding BDE. In the case of acetonitrile, the hydrogen-atom abstraction step involves not only C–H bond cleavage, but also an electronic reorganization on the CN group, whereby the radical becomes partially delocalized. Such an electronic rearrangement is likely to be the origin of the rather high barrier computed for hydrogen-atom abstraction in acetonitrile, although its C–H bond strength is similar to that of the secondary C–H bond of propane.

Alkane hydroxylation—a comparison between theory and experiment: The theoretical findings can be compared with the experimental results collected for alkane hydroxylation by the Fe(tpa) catalyst.[4] Cyclohexane was used in the experiments, and propane is a suitable model for the larger alkane: in both cases secondary C–H bonds are involved in hydrogen-atom abstraction by the high-valent iron–oxo species, and therefore similar barriers are expected for cyclohexane and propane.[54] The principal experimental evidence pointing toward the involvement of an iron(v)–oxo species in alkane hydroxylation is the incorporation of ^{18}O when the reaction is carried out in the presence of $H_2{}^{18}O$. For example, oxidation of cyclohexane with $H_2{}^{16}O_2$ in the presence of labeled solvent ($H_2{}^{18}O$) gives cyclohexanol with about 30% ^{18}O incorporation.

The energy profiles of Figure 10 indicate that hydrogen-atom abstraction from propane leads to recombination with the oxo group (**P-prod1**), but they also show that recombination can involve O2 of the hydroxo ligand (**P-prod2**). Re-

combination with O2 of the hydroxide, which would correspond to the labeled oxygen coming from the solvent, leads to the incorporation of ^{18}O in the alcohol. As explained above, recombination with O2 must involve the doublet potential-energy surface, either through a quartet-to-doublet spin transition on the reactant side or by spin crossing in the vicinity of the transition state. Because the doublet iron(v)–oxo species lies rather high in energy, we favor hydrogen-atom abstraction on the quartet surface and spin transition to the doublet surface in the vicinity of the transition state. On the other hand, recombination with the hydroxide originating from the oxo group, which is derived from H_2O_2, may occur along both the quartet and the doublet potential-energy surfaces. It is expected that the chemical transformation along the quartet potential-energy surface, which corresponds to the ground state of the HO–Fe^{V}=O species, is faster since it involves no spin crossing, and it follows that incorporation of the oxo oxygen atom is preferred over incorporation of the solvent oxygen atom. This result is indeed in agreement with experiment.

Incorporation of labeled oxygen might also involve a different pathway, that is, oxo–hydroxo tautomerization occurring prior to alkane hydroxylation. If this reaction occurs, the oxo group responsible for hydrogen-atom abstractions might contain oxygen derived from water. As discussed above, the tautomerization reaction mediated by a water molecule has a barrier of about 10 kcal mol^{-1}. Importantly, the barrier computed for propane hydroxylation (7 kcal mol^{-1}) is lower than that of the competing tautomerization, that is, incorporation of the oxygen atom originating from hydrogen peroxide should be favored. In light of the accuracy of the present calculations, oxo–hydroxo tautomerization cannot be excluded as a viable pathway accounting for the experimental oservation of solvent incorporation in the product. The exact ratio of incorporation of solvent oxygen cannot be predicted from the present model, because spin crossing is involved and because the calculated energies are subject to an uncertainty of 3–5 kcal mol^{-1}, which, for example, makes it hard to completely disregard the competing tautomerization. It can be concluded that the involvement of the low-spin state (i.e., $S=1/2$) and possibly of oxo–hydroxo tautomerization determine the degree of incorporation of solvent oxygen, while the high-spin state ($S=3/2$) leads only to incorporation of oxygen originating from hydrogen peroxide.

Note that the suggested mechanism of Figure 10 does not involve any long-lived radical intermediates along the reaction pathway. Hydrogen-atom abstraction is in fact followed directly by C–O bond formation. The nascent alkyl radical present at the transition state for hydrogen-atom abstraction must have a very short lifetime, since the next step (rebound step) occurs with zero barrier. The recombination can be compared to the the epimerization process, with an estimated rate of 10^8–10^9 s^{-1}.[55–57] According to transition-state theory, this rate approximately corresponds to a barrier of 6 kcal mol^{-1}. It follows that alkane hydroxylation by the high-valent iron–oxo species occurs with retention of configuration at the carbon atom because epimerization is slower than recombination. This conclusion agrees with experiments showing that the Fe(tpa) catalyst is able to carry out stereospecific hydroxylation of alkanes.[4]

The investigation on the hydroxylation of acetonitrile shows that hydrogen-atom abstraction, that is, the slow step of the reaction, requires a rather high energy barrier. In particular, the computed activation energy ($\Delta G^{\neq}=18.3$ kcal mol^{-1}) is as high as that obtained for methane ($\Delta G^{\neq}=17.0$ kcal mol^{-1}), and much higher than the activation energy for propane ($\Delta G^{\neq}=7$ kcal mol^{-1}). This result confirms the available experimental data showing that hydroxylation of acetonitrile does not compete with substrate oxidation. Indeed the comparable barriers for C–H bond cleavage of methane and acetonitrile suggest that methane hydroxylation may not be experimentally attainable with the Fe(tpa)/H_2O_2 system. Another possible reaction that might occur between acetonitrile and the iron–oxo species is the formation of acetonitrile *N*-oxide. Since the calculations indicate that the transition-state structure corresponding to the N–O bond formation lies rather high in energy (ca. 30 kcal mol^{-1}), this reaction can also be disregarded.

Conclusions

Hybrid DFT was employed to shed light an the reactivity of the high-valent iron–oxo species HO–(tpa)Fe^{V}=O with alkanes. The HO–(tpa)Fe^{V}=O species was previously proposed to be an intermediate in the oxidative catalysis of iron TPA complexes[4,5,1257] aimed at mimicking non-heme iron oxygenases. For example, a similar intermediate is suggested to be involved in the *cis*-dihydroxylation reaction catalyzed by the Rieske-type dioxygenases.[10]

Hydroxylation of methane and propane to methanol and 2-propanol was explored according to the two-step rebound mechanism, which has been widely discussed by other investigators for the heme case.[40,47] The rebound mechanism involves first a hydrogen-atom abstraction generating the alkyl radical and the HO–(tpa)Fe^{IV}–OH species (see Scheme 2), and second recombination of the alkyl radical with one of the hydroxo ligands. Two different spin states are relevant for alkane hydroxylation by HO–Fe^{V}=O: the quartet ($S=3/2$) and the doublet ($S=1/2$) states. The ground state for the HO–Fe^{V}=O species is the quartet, and the doublet lies rather high in energy. However, in the rebound mechanism the doublet potential-energy surface crosses the quartet surface. For both methane and propane, the slow step of the chemical transformations leading to the alcohols is hydrogen-atom abstraction. Due to the weaker secondary C–H bond of propane, hydrogen-atom abstraction for this alkane has a lower barrier than the corresponding reaction for the C–H bond of methane (see Figures 4 and 10). In the case of methane, the transition state associated with hydrogen-atom abstraction decays to the iron(IV)–hydroxo intermediate, which has a very short lifetime; on the doublet surface a zero barrier is computed for the recombination with

the hydroxo ligand. The transition state for hydrogen-atom abstraction from propane leads directly to the product, that is, 2-propanol. Thus, the nascent propyl radical has a very short lifetime, and this accounts for the stereospecific alkane hydroxylation observed experimentally. Although recombination with the hydroxide originating from the oxo ligand is preferred, recombination with the other hydroxo ligand (i.e., that originating from the solvent water) can also occur. This explains the incorporation of oxygen from water in the alcohol, as observed experimentally. It was found that incorporation of solvent oxygen may also involve another competing pathway, that is, oxo–hydroxo tautomerization of HO–(tpa)Fe^{IV}=O occurring prior to alkane hydroxylation.

Finally, the calculations indicate that hydroxylation of the solvent acetonitrile is kinetically inhibited because of the rather high activation barrier associated with hydrogen-atom abstraction, which is computed to be about 10 kcal mol^{-1} higher than that for propane hydroxylation. This agrees with the experimental observation that solvent hydroxylation does not interfere with the hydroxylation of secondary C–H bonds of alkanes.

Acknowledgments

We thank Dr. Megumi Fujita (University of Minnesota, Minneapolis) for useful discussions. We gratefully acknowledge the National Supercomputer Center (Sweden) for generous grants of computer time at the SGI3800. The oxidation catalysis work at the University of Minnesota is supported by the US Department of Energy.

[1] M. Costas, M. P. Mehn, M. P. Jensen, L. Que, Jr., *Chem. Rev.* **2004**, *104*, 939–986.
[2] E. L Solomon, T. C. Brunold, M. L. Davis, J. N. Kemsley, S.-K. Lee, N. Lehnert, F. Neese, A. J. Skulan, Y.-S. Yang, J. Zhou, *Chem. Rev.* **2000**, *100*, 235–349.
[3] P. Nordlund in *Handbook of Metalloproteins* (Eds: I. Bertini, A. Sigel, H. Sigel), Marcel Dekker, New York, **2001**, pp. 461–570.
[4] K. Chen, L. Que, Jr., *J. Am. Chem. Soc.* **2001**, *123*, 6327–6337.
[5] K. Chen, M. Costas, J. Kim, A. K. Tipton, L. Que, Jr., *J. Am. Chem. Soc.* **2002**, *124*, 3026–3035.
[6] K. Chen, M. Costas, L. Que, Jr., *J. Chem. Soc. Dalton Trans.* **2002**, 672–679.
[7] C. Kim, K. Chen, J. Kim, L. Que, Jr., *J. Am. Chem. Soc.* **1997**, *119*, 5964–5965.
[8] R. Y. N. Ho, G. Roelfes, B. L. Feringa, L. Que, Jr., *J. Am. Chem. Soc.* **1999**, *121*, 264–265.
[9] D. T. Gibson, R. E. Parales, *Curr. Opin. Biotechnol.* **2002**, *11*, 235–243.
[10] M. D. Wolfe, J. V. Parales, D. T. Gibson, J. D. Lipscomb, *J. Biol. Chem.* **2001**, *276*, 1945–1953.
[11] M. Sono, M. P. Roach, E. D. Coulter, J. H. Dawson, *Chem. Rev.* **1996**, *96*, 2841–2887.
[12] A. Bassan, M. R. A. Blomberg, P. E. M. Siegbahn, L. Que, Jr., *J. Am. Chem. Soc.* **2002**, *124*, 11056–11063.
[13] P. J. Stevens, F. J. Devlin, C. F. Chablowski, M. J. Frisch, *J. Phys. Chem.* **1994**, *98*, 11623–11627.
[14] a) A. D. Becke, *J. Chem. Phys.* **1993**, *98*, 5648–5652; b) A. D. Becke, *J. Chem. Phys.* **1992**, *96*, 2155–2160; c) A. D. Becke, *J. Chem. Phys.* **1992**, *97*, 9173–9177.
[15] C. Lee, W. Yang, R. G. Parr, *Phys. Rev. B* **1988**, *37*, 785–789.
[16] Jaguar 4.2, Schrödinger, Portland, Oregon, **2000**.
[17] Gaussian 98 (Revision A.9), M. J. Frisch, G. W. Trucks, H. B. Schlegel, G. E. Scuseria, M. A. Robb, J. R. Cheeseman, V. G. Zakrzewski, J. A. Montgomery, R. E. Stratmann, J. C. Burant, S. Dapprich, J. M. Millam, A. D. Daniels, K. N. Kudin, M. C. Strain, O. Farkas, J. Tomasi, V. Barone, M. Cossi, R. Cammi, B. Mennucci, C. Pomelli, C. Adamo, S. Clifford, J. Ochterski, G. A. Petersson, P. Y. Ayala, Q. Cui, K. Morokuma, D. K. Malick, A. D. Rabuck, K. Raghavachari, J. B. Foresman, J. Cioslowski, J. V. Ortiz, B. B. Stefanov, G. Liu, A. Liashenko, P. Piskorz, I. Komaromi, R. Gomperts, R. L. Martin, D. J. Fox, T. Keith, M. A. Al-Laham, C. Y. Peng, A. Nanayakkara, C. Gonzalez, M. Challacombe, P. M. W. Gill, B. G. Johnson, W. Chen, M. W. Wong, J. L. Andres, M. Head-Gordon, E. S. Replogle, J. A. Pople, Gaussian, Inc., Pittsburgh, PA, **1998**..
[18] P. J. Hay, W. R. Wadt, *J. Chem. Phys.* **1985**, *82*, 299–310.
[19] K. Yoshizawa, Y. Shiota, T. Yamabe, *J. Am. Chem. Soc.* **1998**, *120*, 564–572.
[20] S. Shaik, M. Filatov, D. Schröder, H. Schwarz, *Chem. Eur. J.* **1998**, *4*, 193–199.
[21] D. J. Tannor, B. Marten, R. Murphy, R. A. Friesner, D. Sitkoff, A. Nicholls, B. Honig, M. Ringnalda, W. A. Goddard III, *J. Am. Chem. Soc.* **1994**, *116*, 11875–11882.
[22] B. Marten, K. Kim, C. Cortis, R. A. Friesner, R. B. Murphy, M. N. Ringnalda, D. Sitkoff, B. Honig, *J. Phys. Chem.* **1996**, *100*, 11775–11788.
[23] L. A. Curtiss, K. Raghavachari, G. W. Tucks, J. A. Pople, *J. Chem. Phys.* **1991**, *94*, 7221–7230.
[24] L. A. Curtiss, K. Raghavachari, P. C. Redfern, J. A. Pople, *J. Chem. Phys.* **1997**, *106*, 1063–1079.
[25] L. A. Curtiss, K. Raghavachari, P. C. Redfern, J. A. Pople, *J. Chem. Phys.* **2000**, *112*, 7374–7383.
[26] M. R. A. Blomberg, P. E. M. Siegbahn, M. Svensson, *J. Chem. Phys.* **1996**, *104*, 9546–9554.
[27] A. Ricca, C. W. Bauschlicher, Jr., *J. Phys. Chem. A* **1997**, 8949–8955.
[28] P. E. M. Siegbahn, M. R. A. Blomberg, *Chem. Rev.* **2000**, *100*, 421–437.
[29] M. R. A. Blomberg, P. E. M. Siegbahn, *J. Phys. Chem. B* **2001**, *105*, 9375–9386.
[30] P. E. M. Siegbahn, M. R. A. Blomberg, *Annu. Rev. Phys. Chem.* **1999**, *50*, 221–249.
[31] M. R. A. Blomberg, P. E. M. Siegbahn in *Transition State Modeling for Catalysis* (Eds.: D. G. Truhlar, K. Morokuma), American Chemical Society, Washington, DC, **1999**, pp. 49–60.
[32] P. E. M. Siegbahn, *J. Comput. Chem.* **200**1, *22*, 1634–1645.
[33] A. Bassan, Ph.D. Thesis, Stockholm University, Stockholm, **2004**.
[34] D. Quinonero, D. G. Musaev, K. Morokuma, *Inorg. Chem.* **2003**, *42*, 8449–8455.
[35] R. D. J. Froese, S. Humbel, M. Svensson, K. Morokuma, *J. Phys. Chem. A* **1997**, *101*, 227–233.
[36] L. A. Curtiss, P. C. Redfern, B. Smith, L. Radom, *J. Chem. Phys.* **1996**, *104*, 5148–5152.
[37] J.-M. Mouesca, J. C. Chen, L. Noodleman, D. Bashford, D. A. Case, *J. Am. Chem. Soc.* **1994**, *116*, 11898–11914.
[38] D. Harris, G. H. Loew, *J. Am. Chem. Soc.* **1998**, *120*, 8941–8948.
[39] G. H. Loew, D. Harris, *Chem. Rev.* **2000**, *100*, 407–419.
[40] S. Shaik, S. P. de Visser, F. Ogliaro, H. Schwarz, D. Schröder, *Curr. Opin. Chem. Biol.* **2002**, *6*, 556–557.
[41] P. G. Debrunner in *Iron Porphyrins, Vol. III* (Eds.: B. Lever, H. B. Gray), VCH, New York, **1989**, pp. 137–234.
[42] A. Gold, K. Jayaraj, P. Doppelt, R. Weiss, G. Chottard, E. Bill, X. Ding, A. X. Trautwein, *J. Am. Chem. Soc.* **1988**, *110*, 5756–5761.
[43] J. T. Groves, Y.-Z. Han in *Cytochrome P450: Structure, Mechanism, and Biochemistry*, 2nd. ed. (Ed.: P. R. Ortiz de Montellano), Plenum, New York, **1995**, pp. 3–48.
[44] J.-U. Rohde, J.-H. In, M. H. Lim, W. W. Brennessel, M. R. Bukowski, A. Stubna, E. Münck, W. Nam, L. Que, Jr., *Science* **2003**, *299*, 1037–1039.

[45] M. H Lim, J.-U. Rohde, A. Stubna, M. R. Bukowski, M. Costas, R. Y. H. Ho, E. Münck, W. Nam, L. Que, Jr., *PNAS* **2003**, *100*, 3665–3670.
[46] J. Kaizer, E. J. Klinker, N. Y. Oh, J.-U. Rohde, W. J. Song, A. Stubna, J. Kim, E. Münck, W. Nam, L. Que, Jr., *J. Am. Chem. Soc.* **2004**, *126*, 472–473.
[47] F. Ogliaro, N. Harris, S. Cohen, M. Filatov, S. P. de Visser, S. Shaik, *J. Am. Chem. Soc.* **2000**, *122*, 8977–8989.
[48] K. Yoshizawa, Y. Shiota, T. Yamabe, *J. Am. Chem. Soc.* **1999**, *121*, 147–153.
[49] The peculiar geometry of the sextet state (the Fe-O-H angle is almost 180°) is connected to the gas-phase optimization. Geometry optimization in solution gives a structure with the same energy, but with an FeOH angle similar to those of the lower spin states.
[50] P. Gütlich, A. Hauser, H. Spiering, *Angew. Chem.* **1994**, *106*, 2109–2141; *Angew. Chem. Int. Ed. Engl.* **1994**, *33*, 2024–2054.
[51] P. E. M. Siegbahn, *J. Biol. Inorg. Chem.* **2001**, *6*, 27–45.
[52] M. L. Coote, *J. Phys. Chem. A* **2004**, *108*, 3865–3872.
[53] M. Saeys, M.-F. Reyniers, G. B. Marin, V. Van Speybroeck, M. Waroquier, *J. Phys. Chem. A* **2003**, *107*, 9147–9159.
[54] The computed C–H bond dissociation energies of cyclohexane and propane are 93.6 and 92.7 kcal mol^{-1}, respectively.
[55] A. M. Khenkin, A. E. Shilov, *New J. Chem.* **1989**, *13*, 659–667.
[56] P. D. Bartlett, R. E. Pincock, J. H. Rolston, W. G. Schindel, L. A. Singer, *J. Am. Chem. Soc.* **1965**, *87*, 2590–2596.
[57] P. J. Krusic, P. Meakin, J. P. Jesson, *J. Phys. Chem.* **1971**, *75*, 3438–3453.

Received: April 21, 2004
Published online: December 3, 2004

